Optics Communications 506 (2022) 127610

Contents lists available at ScienceDirect

Optics Communications

journal homepage: www.elsevier.com/locate/optcom

High-precision beam array scanning system based on Liquid Crystal Optical Phased Array and its zero-order leakage elimination

Chengmiao Wang [a,b], Qidong Wang [a,*], Quanquan Mu [a,b], Zenghui Peng [a,b]

[a] State Key Laboratory of Applied Optics, Changchun Institute of Optics, Fine Mechanics and Physics, Chinese Academy of Sciences, Changchun, 130033, PR China

[b] Center of MaterialScience and OptoelectronicsEngineering, University of Chinese Academy of Sciences, Beijing, 100049, China

ARTICLE INFO

Keywords:
Liquid crystal optical phased array
Beam splitting
Gerchberg–Saxton algorithm
Zero-order light leakage

ABSTRACT

In order to improve the scanning efficiency of lidar, a set of high precision scanning system with 40 × 40 sub-beams is established, in which a liquid crystal optical phased array is used to load the phase calculated by Gerchberg–Saxton(GS) algorithm to split the incident plane wave. Technically, the imperfections of GS algorithm often lead to problems such as sidelobes and uneven intensity of output spots, which eventually result in poor pointing accuracy of sub-beams and low scanning resolution of lidar. To solve those problems, we propose an optical method rather than the classical algorithm optimization methods, which restricts the preset sub-beams to the diffraction limit to unify the actual sub-spot morphology and ensure high pointing accuracy. In this way, the standard deviation of pointing error eventually decreases from 42 μrad to 16 μrad. In the aspect of eliminating zero-order leakage, the zero-order light leakage cannot be separated by the conventional tilt method in the case that the spatial spectrum span of the generated beam array exceeds the cut-off frequency. Concerning this issue, a novel zero-order leakage elimination method is proposed to avoid zero-order leakage by splicing two half beam array of adjacent diffraction orders on both sides of the cut-off frequency. Meanwhile, the intensity correction is carried out to achieve leakage avoidance without damaging the intensity uniformity of the beam array.

1. Introduction

LiDAR or Light Detection and Ranging is an active remote sensing system which uses laser beam to search and track the target and accurately measure the azimuth, distance and speed of the target [1–3]. Due to the limitation of mechanical structure, the traditional mechanical scanning lidar is gradually difficult to meet the requirements of high speed and light weight. In contrast, lidar based on non-mechanical device design has many advantages, such as lower size, weight and power (SWaP), programmable, and able to realize agile scanning [4–6]. Therefore, optical phased array lidar is an important development trend of lidar at present.

Liquid Crystal Optical Phased Array (LCOPA) is a relatively mature technique for scanning single beam with extremely high precision [7–11]. However, the existing large field of view scanning radars often need to give consideration to the scanning efficiency while ensuring the pointing accuracy, which is difficult to achieve for the single beam scanning system with a frame frequency of up to 1 kHz [12–14]. Based on this limitation, multi-beam parallel scanning has gradually become a preferred method to improve the scanning speed in beam scanning system. Compared with the single beam scanning system with the same frame frequency, its scanning efficiency will be improved by several orders of magnitude. Among various beam array generation methods, such as source-microlens array and Dammann Grating, Liquid Crystal Optical Phased Array has an obvious advantage in fine-tuning the pointing position of the beam, so it is more conducive to ensure the pointing accuracy of the output light in actual system where the system aberration and adverse environmental factors exist.

In this paper, an ultrafast beam array scanning system with 40 × 40 sub-beams, scanning range of 15° and scanning interval of 1.1 mrad is set up, whose scanning frame rate is about 1 kHz and the average pointing error of sub-beams is expected to be less than 30 μrad. In the system, GS algorithm is used to calculate the beam splitting phase, LCOPA is used to perform static beam splitting and fine-tune the pointing position of the sub-beams, and Liquid Crystal Polarizing Gratings (LCPGs) are used to realize fast scanning between discrete large angles. In order to solve the problem that the imperfection of GS algorithm leads to sidelobes and uneven intensity of sub-beams, which further affects the pointing accuracy, we propose an optical optimization method to unify the spot morphology by limiting the preset sub-spot to the diffraction limit. To solve the problem that zero-order leakage cannot be separated when the spatial frequency span of the beam array is larger than the cut-off frequency, we propose a zero-order leakage avoidance method

* Corresponding author.
E-mail address: qdwang@ciomp.ac.cn (Q. Wang).

https://doi.org/10.1016/j.optcom.2021.127610
Received 26 August 2021; Received in revised form 1 November 2021; Accepted 2 November 2021
Available online 6 November 2021
0030-4018/

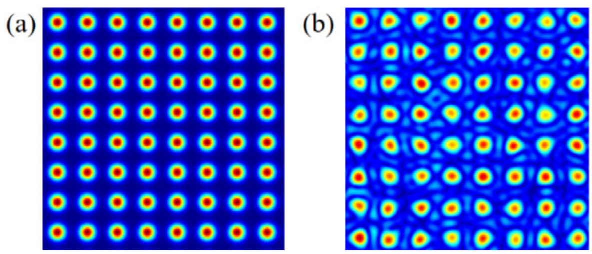

Fig. 1. The spot array of GS algorithm. (a) The preset array; (b) Computed output array.

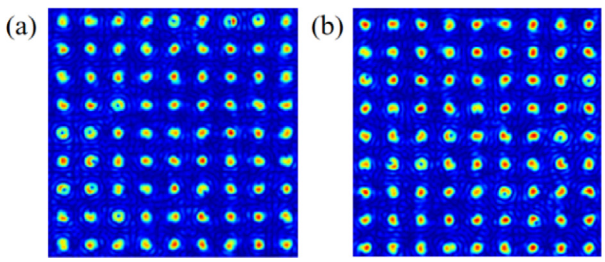

Fig. 2. Computed output spot array of the optimization scheme of GS algorithm. (a) Phase-mixture algorithm; (b) Intensity-phase separate constraint algorithm.

by splicing adjacent diffraction orders on both sides of the cut-off frequency barrier. In conjunction with the intensity correction process of the preset sub-beams, the perfect reproduction of the beam array without affecting the intensity uniformity is finally realized.

2. Diffraction limit constraint of sub-beams

GS algorithm [15] is a cyclic optimization phase solution method based on Fourier transform and inverse transform, which has a wide range of applications in phase retrieval [16–18] and beam shaping [19,20]. Given the distribution of the complex amplitude distribution of the input light and the preset amplitudes of the output light, GS algorithm can be used to calculate the additional phase-only transmittance function which is needed to achieve the desired diffraction effect. Beam splitting, as a special branch of beam shaping, can also be realized by GS algorithm. In our work, the total width of the 40 × 40 beam array is set as 2.5°, so the angular interval between adjacent sub-beams is about 1.1 mrad. Under the condition that the filling factor is set at 0.5, the preset spot array and the computed output array of GS algorithm are shown in Fig. 1.

It can be seen from Fig. 1 that the computed output spot array contains many sidelobes and their morphology varies greatly, which is caused by the imperfection of GS algorithm. For this kind of mathematically unresolvable phase problem, multiple sidelobes and uneven intensity are common phenomena in the calculation results. Since the invention of GS algorithm, a large number of relevant scholars have tried to make the computed output intensity distribution closer to the preset intensity distribution from the perspective of algorithm improvement, such as phase-mixture algorithm and intensity-phase separate constraint algorithm [21,22]. Fig. 2 shows the effect of beam array generated by these two improved algorithms of GS.

In all of this algorithmic optimization work, the improvement of spot quality is mostly evaluated by the energy utilization or energy uniformity. However, the work of evaluating spot quality by pointing accuracy of sub-beams is rarely reported. Although these existing schemes can suppress sidelobes visually, there are still differences in spot morphology and the maximum pointing error is close to 40 μrad. In terms of pointing accuracy, which is a new evaluation index closer to the practical application of lidar, the generation method of beam array still needs to be further improved.

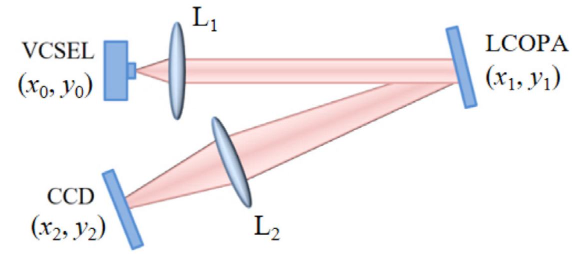

Fig. 3. Sketch diagram of beam splitting path and coordinate parameter setting.

To solve this problem, we propose an optical optimization method based on the improved algorithm of GS. Assume that the schematic diagram of beam splitting path is shown in Fig. 3.

In Fig. 3, the aperture of the laser source is about tens to hundreds of microns, and its output complex amplitude is set as $\widetilde{E}_0\left(x_0, y_0\right)$. After passing through the collimating lens L_1, the spatial spectrum of the original complex amplitude on the back focal plane is denoted as $\widetilde{G}_1\left(f_x, f_y\right) = \mathrm{FT}\left[\widetilde{E}_0\left(x_0, y_0\right)\right]$, in which the function FT stand for Fourier transform. Since the aperture of the light source is much smaller than the aperture of L_1, the transmitted light of L_1 is collimated well enough so that it can be approximately considered that the complex amplitude at the LCOPA panel is still equal to that at the back focal plane of L_1, which can be written as $\widetilde{G}_1\left(x_1/\lambda F_1, y_1/\lambda F_1\right)$, where F_1 is the focal length of lens L_1. The beam splitting phase obtained by GS algorithm is denoted as $\varphi_{\mathrm{GS}}(x_1, y_1)$. Since the default incident light in the calculation process of GS algorithm is standard plane wave, the complex amplitude obtained by far-field diffraction in theory is the spectrum of the beam splitting phase, denoted as $\widetilde{G}_2(f_x, f_y) = \mathrm{FT}\left[\exp\left(i\varphi_{\mathrm{GS}}\left(x_1, y_1\right)\right)\right]$. However, the actual incident light of LCOPA deviates from the ideal plane wave. After passing through the Fourier lens L_2, the actual diffraction wave at the back focal plane is shown in Eq. (1)

$$\widetilde{E}_2\left(f_{x2}, f_{y2}\right) = \mathrm{FT}\left[\widetilde{G}_1\left(\frac{x_1}{\lambda F_1}, \frac{y_1}{\lambda F_1}\right) \cdot \exp\left(i\varphi_{\mathrm{GS}}\left(x_1, y_1\right)\right)\right] \tag{1}$$

Based on the properties of the double Fourier transform, the complex amplitude can be transformed into Eq. (2)

$$\widetilde{E}_2\left(f_{x2}, f_{y2}\right) = -\lambda F_1 \widetilde{E}_0\left(\lambda F_1 f_{x2}, \lambda F_1 f_{y2}\right) * \widetilde{G}_2\left(f_{x2}, f_{y2}\right) \tag{2}$$

After the spectral coordinates are transformed into spatial coordinates, Eq. (2) can finally be written as the proportional relation, as shown in Eq. (3).

$$\widetilde{E}_2\left(\frac{x_2}{\lambda F_2}, \frac{y_2}{\lambda F_2}\right) \propto -\widetilde{E}_0\left(\frac{F_1}{F_2}x_2, \frac{F_1}{F_2}x_2\right) * \widetilde{G}_2\left(\frac{x_2}{\lambda F_2}, \frac{y_2}{\lambda F_2}\right) \tag{3}$$

It can be seen that the final diffraction complex amplitude distribution is proportional to the convolution of the light source image and the calculated output diffraction pattern. In the technique of beam shaping using GS algorithm, the spectrum distribution width of the preset diffraction pattern is usually much larger than the size of the light source image, thus, the result of above-mentioned convolution process is to smooth and blur the whole pattern. Different from beam shaping, the preset output pattern of beam splitting is a special lattice distribution rather than a continuous distribution in wide range. If each sub-spot is no longer preset as a moderate size in Fig. 4(a), but as a light point with a width far less than that of the light source image, the beam splitting pattern calculated by GS can be approximated to an array of δ functions. Then the convolution result can be regarded as the copy of the light source image at each light point, and the actual sub-spot morphology tends to be uniform.

However, in the calculation process of the output intensity distribution, the sub-beam width cannot break through the diffraction limit, so the preset angular width of the sub-spot should be changed to the

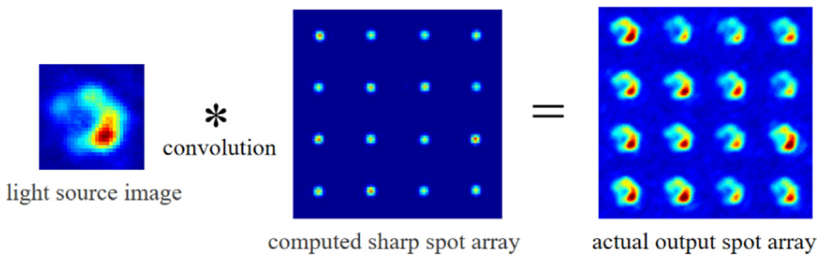

Fig. 4. Schematic diagram of the actual output array when the preset sub-beam reaches the diffraction limit.

width corresponding to the diffraction limit of $2.44\lambda/D$. The aperture of the incident collimating beam is 6 mm and the wavelength of the light source is 910 nm. Based on this, the preset angular width of the sub-beam is about 0.37 mrad and the full width at half maximum is $1.03\lambda/D = 0.16$ mrad, which is more significant in comparison with the image size of the light source. Meanwhile, the aperture of the light source D_s was adjusted to 100 μm and the focal length of the Fourier lens F_2 was set to 200 mm. Therefore, the angular width of the light source image is $D_s/F_2 = 0.5$ mrad. The convolution diagram of the actual beam array is shown in Fig. 4.

Although the preset width of the sub-spot cannot perfectly meet the condition that it is far less than the image width of the light source, the local shot of the actual output array in Fig. 4 shows that the morphology of the sub-spot is still basically the same as that of the light source image.

The advantage of setting the sub-spot size in this way is quite obvious: when the size of the preset sub-spots is reduced to the diffraction limit, the computed output sub-spots will lose morphology details. As a whole, the spot array presents as multiple dots with only different intensity, rather than a group of sub-spots in Fig. 2 with different complicated morphologies. In this ideal case, the computed output beam array only determines the position of the actual sub-spots and their morphologies are completely determined by the morphology of light source image. Finally, the sub-spots have similar morphologies to each other, and the problems of different spot shapes and low pointing accuracy caused by the imperfection of GS algorithm can be effectively solved.

3. Zero order leakage elimination

In the process of spatial light modulation by using LCOPA, there is always an obvious bright spot at the center of the far-field diffraction pattern, whose brightness does not change significantly with the change of the modulation phase. This is called the zero-order leakage phenomenon. Since there are pixel gaps between adjacent pixels of LCOPA and the light absorption rate cannot reach 1, the light reflected from pixel gap diffracts to form leakage spots.

Assuming that the pixel period of two-dimensional LCOPA is d and the pixel width is a, as shown in Fig. 5. The white area is the interior of the pixel, that is, the active area of phase modulation, while the pixel gap is the gray area, also known as the dead space.

Without considering the influence of the overall aperture of LCOPA, the optical transmittance function of the dead space is shown in Eq. (4) [23].

$$t_{DS} = \left[\mathrm{rect}\left(\frac{x}{d},\frac{y}{d}\right) - \mathrm{rect}\left(\frac{x}{a},\frac{y}{a}\right)\right] * \frac{1}{d^2}\mathrm{comb}\left(\frac{x}{d},\frac{y}{d}\right)\cdot A_{DS}\exp\left(i\varphi_{DS}\right) \tag{4}$$

In which A_{DS} is the amplitude reflectance constant of dead space and $0< A_{DS}<1$. φ_{DS} is the phase function of dead space. The expressions of rect and comb functions are shown in Eqs. (5) and (6), respectively.

$$\mathrm{rect}(x) = \begin{cases} 1 & |x| < 0.5 \\ 0.5 & |x| = 0.5 \\ 0 & |x| > 0.5 \end{cases} \tag{5}$$

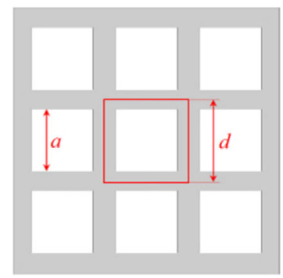

Fig. 5. Schematic diagram of the pixel gap in LCOPA.

$$\mathrm{comb}(x,y) = \sum_{M,N=-\infty}^{+\infty}\delta(x-M,y-N) \tag{6}$$

For incident plane wave with intensity of 1, the far-field diffraction pattern of dead space light is shown in Eq. (7).

$$T_{DS} = \left[\mathrm{sinc}\left(df_x,df_y\right) - \mu\mathrm{sinc}\left(af_x,af_y\right)\right]\cdot\mathrm{comb}\left(df_x,df_y\right) * \mathrm{FT}\left[A_{DS}\exp\left(i\varphi_{DS}\right)\right] \tag{7}$$

Where μ is called the filling factor of LCOPA and $\mu = a^2/d^2$. It can be seen that the dead zone leakage is distributed in an array with an interval frequency of $1/d$. If the phase of the dead space is approximately constant, the dead space leakage is the strongest when $f_x = f_y = 0$, that is, the zero-order leakage. In fact, the dead space phase is affected by the modulated phase and varies from place to place. Theoretically, the intensity of zero-order light emission can be reduced by controlling the active area phase [24]. However, due to the calculation complexity of indirect control of the dead space phase, it is difficult to achieve complete suppression of zero-order light in practical application.

In the beam shaping technology, the zero-order leakage can be blocked by high-pass filter when the far-field diffraction beam has no energy distribution near the center of the space spectrum. In our work, the width of the zero-order leakage spot is close to that of the sub-spot constrained by the diffraction limit. Referring to the relationship between spot width and spot spacing in Fig. 4, it can be seen theoretically that zero-order leakage can be contained in the sub-beam gap and be independently blocked. However, the energy of effective light is divided into 1600 parts, actually making the energy of zero-order light leakage far stronger than that of nearby sub-beams, as shown in Fig. 6.

Fig. 6 shows a high-brightness cross image of zero-order leakage by square hole diffraction. Excessive light leakage intensity makes the surrounding diffraction secondary also reached the saturation intensity of receiving CCD and connected as a whole, that is, star effect. The effect makes the two rows of sub-beams passing near the center be affected or even submerged, so the zero order cannot be eliminated by occlusion method without affecting the transmission of signal light.

Another common scheme to eliminate zero-order light leakage is to separate the effective light from the light leakage by attaching tilt or defocus phase to LCOPA [25], as shown in Fig. 7.

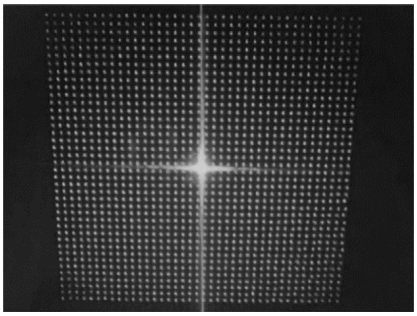

Fig. 6. Zero-order leakage in the beam array.

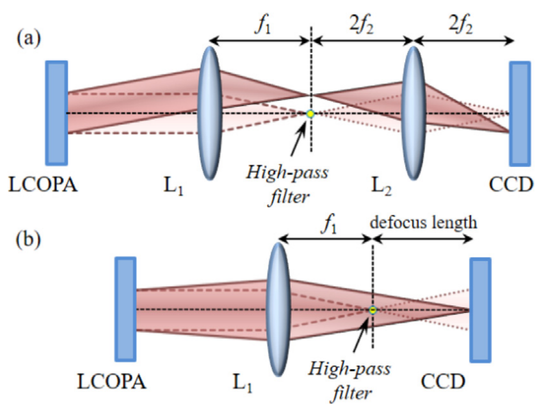

Fig. 7. Schematic diagram of zero-order leakage elimination with additional phase modulation. (a) Tilt method; (b) Defocus method.

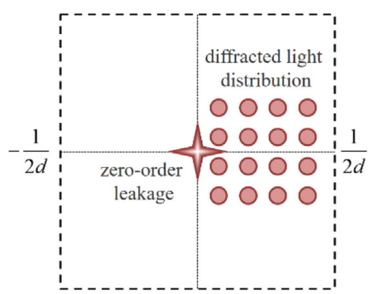

Fig. 8. Schematic diagram of constrained spatial spectrum of modulated light due to avoidance of zero-order leakage.

The main problem of defocus method is that the high-pass filter will still disturb the effective light. When the additional defocus amount is small, the discrete amount Δ in Fig. 7 is insufficient and there will still be a diffuse image of the block on the defocus plane, which will lead to the decline of Signal-to-Noise Ratio in the neighborhood. When the defocusing amount is too large, it will seriously increase the volume of the system and affect the convenience of application. The main problem of the tilt method is that the additional tilt quantity is limited by the cut-off frequency $1/2d$. The spatial frequency range in which the diffracted light is located must deviate from the zero of the spatial frequency and cannot exceed cut-off frequency. Therefore, the spatial frequency span of the diffraction pattern must be less than $1/2d$, which severely limits the ability of LCOPA to achieve diffraction with wide spatial spectrum, as shown in Fig. 8.

To solve above problem, a new zero-order leakage elimination method is proposed based on diffraction characteristics, which is equivalent to moving part of the diffraction pattern out of the cut-off frequency barrier. The basic theory is as follows. When LCOPA is loaded with any mathematically closely sampled phase surface $\varphi(x, y)$, the surface will be discretized and transformed into a step-like distribution. In view of this effect, the phase modulation factor generated by LCOPA can be written as Eq. (8) and the light distribution after far-field diffraction can be written as Eq. (9).

$$\exp\left[i\varphi'(x,y)\right] = \exp\left[i\varphi(x,y)\right]\cdot\frac{1}{d^2}\mathrm{comb}\left(\frac{x}{d},\frac{y}{d}\right) * \mathrm{rect}\left(\frac{x}{a},\frac{y}{a}\right) \cdot \mathrm{rect}\left(\frac{x}{L},\frac{y}{L}\right) \tag{8}$$

$$G'\left(f_x,f_y\right) \propto \mathrm{sinc}\left(Lf_x,Lf_y\right) * \left[G\left(f_x,f_y\right) * \mathrm{comb}\left(df_x,df_y\right) \cdot \mathrm{sinc}\left(af_x,af_y\right)\right] \tag{9}$$

In Eq. (9), The point spread function sinc(Lf_x, Lf_y) obscures the diffraction pattern. $G(f_x, f_y)$ represents the far-field diffraction spatial spectrum of the ideal phase surface and $G(f_x, f_y)$ = FT[exp($i\varphi(x, y)$)]. The convolution with comb(df_x, df_y) represents that the ideal diffraction pattern will be periodically copied to the region with higher spatial frequency at a spatial frequency interval of 1/d, that is, the secondary diffracted light. The diffraction efficiency factor sinc(af_x, af_y) represents the intensity envelope surface that slowly weakens as the spatial spectrum coordinates deviate from the center.

The zero-order light leakage elimination method is realized by diffraction order splicing based on GS algorithm. The flow diagram of the process is shown in Fig. 9.

In Fig. 9, the initial beam array disturbed by zero-order light leakage is firstly divided into upper half region A and lower half region B, then the preset light intensity distribution of A and B were moved down and up by $1/2d$, respectively. According to the comb function in Eq. (9), after the new regions A' and B' are formed inside the cut-off frequency, there will be a replication of A' at region C outside the upper cut-off frequency. The position C is further away from the center of the spatial frequency coordinates. According to the diffraction efficiency factor, the intensity at C should be weaker than the original light intensity in region A'. However, if the default light intensity in A' is artificially increased, the intensity in C may be equal to that in B'. As parts of two adjacent diffraction orders, region C and B' are spliced together to form a complete spot array on both sides of the cut-off frequency, which is no longer disturbed by light leakage.

In order to make the intensity uniformity of the spliced spot array basically the same as that of the original spot array, the light intensity needs to be quantitatively corrected according to the diffraction efficiency factor. As a matter of convenience, the quantitative intensity correction process is set before the positions of regions A and B are exchanged. The specific steps are shown in Fig. 10.

The actual diffraction intensity at the coordinate (f_x, f_y) is the product of the preset intensity and the diffraction efficiency factor sinc(af_x, af_y), resulting in the actual diffractive light being slightly weaker at the edge. To solve this problem, The light intensity correction process in Fig. 10 is mainly divided into three steps:

1. Lateral intensity modulation. In order to make the actual intensity of each sub-beam uniform in the lateral direction, edge enhancement is directly carried out on the preset light distribution, that is, the preset complex amplitude G(f_x, f_y) of the sub-beam should be divided by the diffraction efficiency factor sinc(af_x).
2. Longitudinal intensity modulation. In order to make the actual intensity of each sub-beam uniform in the longitudinal direction, the preset light distribution also needs to be divided by the diffraction efficiency factor in f_y direction. However, it should be noted that the enhanced beam array is equivalent to the initial beam array moving up the cut-off frequency $1/2d$, and the diffraction efficiency factor in the denominator should be sinc[$a(f_y+1/2d)$]. In this case, the complex amplitude distribution is changed to Eq. (10).

$$G'\left(f_x,f_y\right) = \frac{G\left(f_x,f_y\right)}{\mathrm{sinc}\left(af_x\right)\cdot\mathrm{sinc}\left[a\left(f_y+1/2d\right)\right]} \tag{10}$$

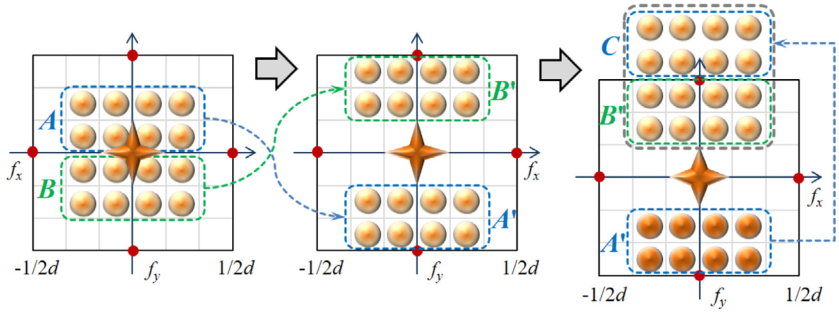

Fig. 9. Flow diagram of the diffraction order splicing.

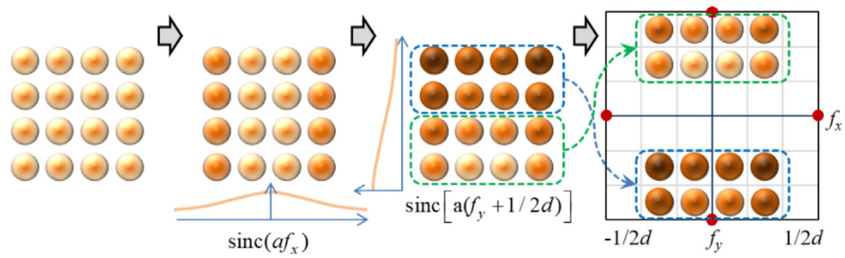

Fig. 10. Schematic diagram of quantitative intensity correction in diffraction order splicing method.

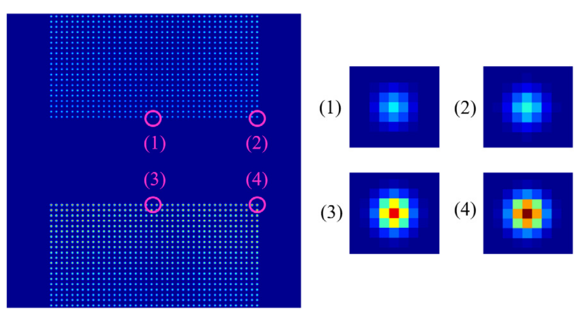

Fig. 11. The preset light intensity after quantitative intensity correction.

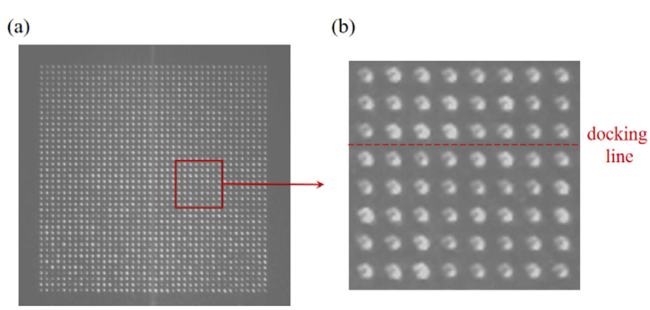

Fig. 12. Beam splitting effect using diffraction order splicing method. (a) Overall effect; (b) The local effect at the docking position.

3. The upper and lower halves are interchanged. The upper half of the complex amplitude $G'(f_x,\ f_y)$ is shifted down by $1/2d$ and the lower half is shifted up by $1/2d$. The results of the interchange can be expressed in Eq. (11). The definition of the sign function is shown in Eq. (12).

$$G''\left(f_x, f_y\right) = G'\left(f_x, f_y - \operatorname{sgn}\left(f_y\right) \cdot 1/2d\right) \tag{11}$$

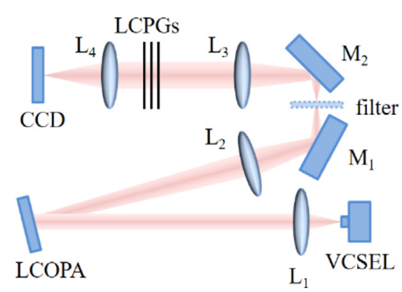

Fig. 13. Schematic diagram of the beam array scanning system.

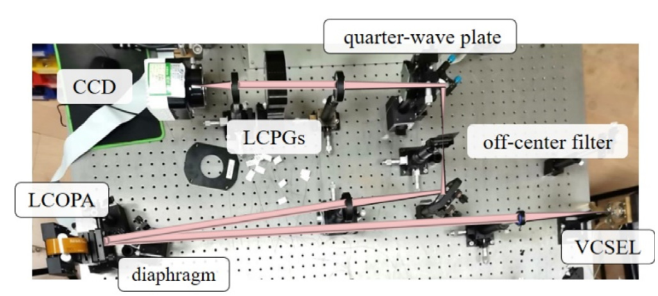

Fig. 14. Physical image of the beam array scanning system.

$$\operatorname{sgn}(x) = \begin{cases} -1 & x < 0 \\ 0 & x = 0 \\ 1 & x > 0 \end{cases} \tag{12}$$

After the correction of the above three steps, the preset light intensity is changed to the form shown in Fig. 11.

It can be seen that the preset intensity of each sub-beam is not the same after the quantitative intensity correction. Especially in f_y direction, the diffraction efficiency factor becomes an asymmetrical structure due to the position translation, leading to a more obvious difference between the preset sub-beams in f_y direction. In theory, the

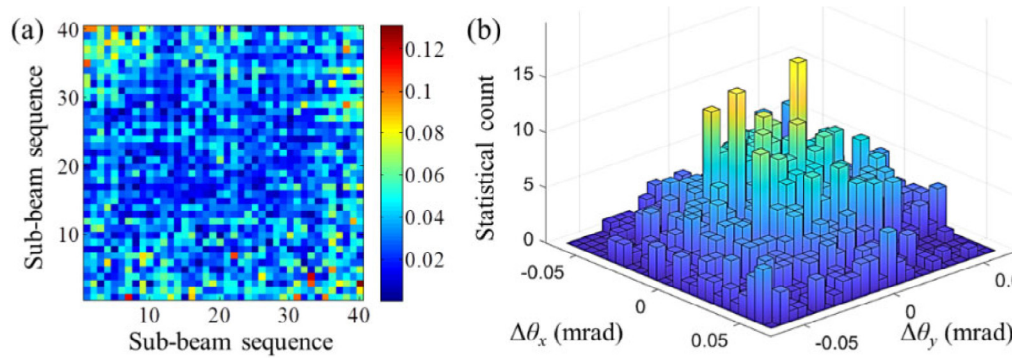

Fig. 15. The pointing accuracy testing results of the sub-beams without morphology unification. (a) Pointing error of each sub-beam, unit: mrad; (b) Histogram of pointing error distribution.

ordinary zero-order leakage elimination method with additional tilted phase also needs the intensity correction, otherwise the beam array will also have a small overall intensity difference, but this difference is acceptable due to its small spatial frequency offset. For the diffraction order splicing method proposed in this paper, the spatial frequency offset of the beam array increases greatly and 50% of the spatial spectrum components exceed the cut-off frequency. Therefore, the intensity correction process in this method is more necessary in the case that the diffraction efficiency factor at different positions varies greatly.

For LCOPA in this work, the pixel width a is 0.9 times the pixel period d. After adjusting the diffraction efficiency factor used for intensity correction, the beam splitting effect is shown in Fig. 12.

Compared with Fig. 6, the zero-order leakage in Fig. 12 has been successfully separated and the diffraction splicing method has successfully reached the expected goal. After the intensity correction, the intensity of some sub-beams still fluctuates slightly, but the overall trend of intensity variation will no longer exist.

The intuitive effect achieved by the above method is quite similar to the overall shift of the spot array by $1/2d$ in the spatial frequency domain, but this method is fundamentally different from the simple tilt method. On the one hand, the upper and lower half regions realized by the method are not the same diffraction order and the array beam outside the upper cut-off frequency can only be controlled indirectly by setting the corresponding main diffraction order. On the other hand, due to the necessity of the intensity correction, the modulation phase used in this method needs to be recalculated by GS algorithm rather than obtained by adding an additional tilt to the original beam splitting phase. Considering the above two reasons, diffraction order splicing method should be regarded as an independent zero-order light leakage elimination method, instead of a derivative usage of the tilt method.

Diffraction order splicing method can eliminate the zero-order leakage of the light distribution whose frequency domain width is nearly twice the cut-off frequency, and its application scope is not limited to the beam splitting task in this paper, but is applicable to the whole field of beam shaping. Limited by the splicing and intensity correction process, the light energy utilization rate of the beam array decreases slightly compared with that before zero-order leakage elimination. Therefore, this method is more suitable for the beam scanning system with less strict requirements on energy loss.

4. Experimental apparatus and measurement

A beam array scanning system is built after above optical path setting details are confirmed. Its schematic diagram is shown in Fig. 13 and the physical image is shown in Fig. 14.

In the system, a Vertical Cavity Surface Emitting Laser (VCSEL) with small optical waist size and high power density is used as the light source [26], whose wavelength is 910 nm. Its aperture is processed into 100 μm, which can not only meet the conditions that the light source image is much larger than the diffraction limit width of sub-beams, but also avoid local overlap of adjacent spots. The aperture of the emitted light is limited to 6 mm after being collimated by L_1 with a focal length of 200 mm. The LCOPA (Produced by meadowlark company of the United States, model: SN3561) with 512 × 512 pixels and 15 μm pixel pitch modulates the incident plane wave to generate a beam array in the far field. With the same focal lengths of 300 mm, L_2 and L_3 constitute a 4F system together. An off-center filter diaphragm is installed on the space spectrum surface where the focal points of the two overlap, whose function is to block the zero-order light leakage and let the off-center beam array generated by the above zero-order elimination method pass through. After the lens L_3, a cascaded liquid crystal polarizing grating [27] is placed to carry out discrete beam steering with large angles. The two-dimensional discrete angles can be set as ±1.25°, ±3.75° and ±6.25°. The interval between adjacent angles is 2.5°, which is exactly equal to the total width of the beam array generated by LCOPA. The focal length of L_4 is 100 mm, and a CCD with a large receiver panel width is placed on its rear focal plane to observe the beam scanning with a full field angle of 15°.

After the interference of zero-order light leakage was successfully removed, the quantitative measurement of pointing accuracy can be carried out. The preliminary testing results of the sub-beams without morphology unification are shown in Fig. 15 and the further testing results of the sub-beams after morphology unification are shown in Fig. 16.

By comparing Fig. 16 with Fig. 15, it can be seen that after the preset sub-beam width is constrained to the diffraction limit and the actual sub-beam morphology is similar to the light source image, the pointing error of most sub-beams decreases obviously. In a statistical sense, the distribution peak of the error distribution histogram become significantly narrowed and sharp, and the standard deviation of pointing error is compressed from 42 μrad to 16 μrad. The expected target of pointing accuracy is basically achieved. If the condition that the diffraction limit size of sub-beams is much smaller than the light source image could be more strictly satisfied, the morphology similarity of the sub-spot would be further improved and the pointing error might be further compressed.

Finally, a beam array with 40 × 40 sub-beams and 1.1 mrad sub-beam interval was incident into LCPGs to realize the parallel scanning. With the help of LCPGs, the center position of the beam array can be scanned to 36 two-dimensional coordinates corresponding to 6 angles of ±1.25°, ±3.75° and ±6.25°. The scanning effect of the pictures taken at some of its positions is shown in Fig. 17.

Intuitively, the uniformity of the beam array decreases slightly in the large field of view mode, which is due to the limitation of computer screen resolution. The actual uniformity of the beam array will not be affected by LCPGs. In Fig. 17(d), the beam array splicing can be achieved without seams, overlaps and lateral dislocations, which meets the basic requirements of uniform scanning of the target field of view. In the case of 1 ms per frame, above prototype can achieve the ultra-fast scanning rate of 1.6×10^7 units per second, which is unmatched by any single beam scanning instrument.

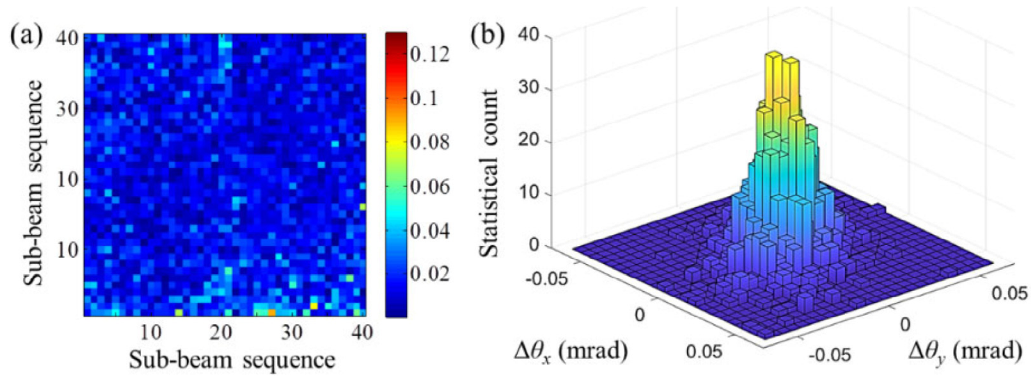

Fig. 16. The pointing accuracy testing results of the sub-beams after morphology unification. (a) Pointing error of each sub-beam, unit: mrad; (b) Histogram of pointing error distribution.

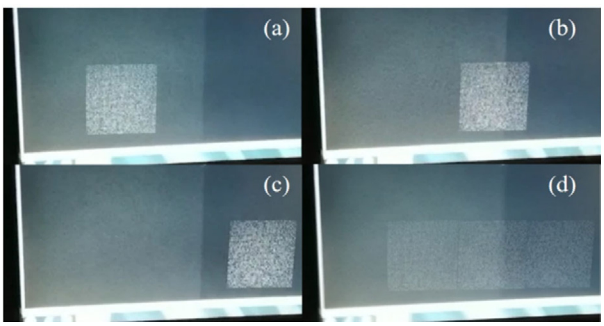

Fig. 17. The overall scanning effect of the beam array. (a) Scan position of row 5, column 2; (b) Scan position of row 5, column 3; (c) Scan position of row 5, column 4; (d) Splicing effect of column 2, 3, 4 in row 5.

5. Conclusion

In this paper, a beam array scanning system with both high scanning speed and high pointing accuracy is set up, which uses LCOPA to load the beam splitting phase calculated by GS algorithm to diffract the single collimating plane wave into a beam array with 40 × 40 sub-beams. Aiming at the problem that the imperfection of GS algorithm leads to different sub-spot shapes and low pointing accuracy, an improved optical method is proposed, in which the preset spot size is constrained to the diffraction limit size, which is much smaller than the width of the light source image. Under the premise that the actual spot morphology is the convolution of the preset sub-spot morphology and the light source image, the actual spot morphology tends to be unified and the standard deviation of pointing error decreases from 42 μrad to 16 μrad.

In terms of zero-order leakage elimination, for the diffraction patterns whose frequency span exceeds the cut-off frequency, the traditional tilt and defocus methods cannot effectively eliminate zero-order leakage without affecting the beam array quality. Basing on the diffraction characteristics of LCOPA pixel structure, a new diffraction order splicing method is proposed to make each half regions of adjacent diffraction orders splice together to form a complete beam array at the cut-off frequency. Finally, with the fine correction of intensity, the avoidance of zero-order light leakage can be realized perfectly.

Funding

This work was sponsored by the National Natural Science Foundation of China (11974345, 61975202, U2030101 and 11604327) and the Science Foundation of State Key Laboratory of Applied Optics, PR China.

Declaration of competing interest

The authors declare that they have no known competing financial interests or personal relationships that could have appeared to influence the work reported in this paper.

Acknowledgment

This work was supported by the National Science Foundation of China and State Key Laboratory of Applied Optics, Changchun Institute of Optics, Fine Mechanics and Physics, Chinese Academy of Sciences.

References

[1] C. Peng, Z. Yu, Modeling analysis for positioning error of mobile lidar based on multi-body system kinematics, Intell. Autom. Soft Comput 25 (4) (2019) 827–834.
[2] S.E. Reutebuch, A. Hans-Erik, R.J. Mcgaughey, Light detection and ranging (LIDAR): An emerging tool for multiple resource inventory, J. Forestry -Washington 103 (6) (2005) 286–292.
[3] N.L. Seldomridge, J.A. Shaw, K.S. Repasky, Dual-polarization lidar using a liquid crystal variable retarder, Opt. Eng. 45 (10) (2006) 106202.
[4] P.F. Mcmanamon, T.A. Dorschner, D.L. Corkum, L.J. Friedman, Optical phased array technology, Proc. IEEE 84 (2) (1996) 268–298.
[5] P.F. Mcmanamon, P.J. Bos, M.J. Escuti, J. Heikenfeld, S. Serati, H. Xie, E.A. Watson, A review of phased array steering for narrow-band electrooptical systems, Proc. IEEE 97 (6) (2009) 1078–1096.
[6] D. Vettese, Microdisplays: Liquid crystal on silicon, Nat. Photonics 4 (11) (2010) 752–754.
[7] D. Engström, J. Bengtsson, E. Eriksson, M. Goksör, Improved beam steering accuracy of a single beamwith a 1D phase-only spatial light modulator, Opt. Express 16 (22) (2008) 18275–18287.
[8] L. Kong, Z. Ying, S. Yan, J. Yang, Beam steering approach for high-precision spatial light modulators, Chin. Opt. Lett 8 (11) (2010) 1085–1089.
[9] C. Wang, Z. Peng, Y. Liu, S. Li, Z. Zhao, W. Chen, Q. Wang, Q.M. Mu, Radial sub-aperture coherence method used to achieve beam steering with high precision and stability, Opt. Express 27 (5) (2019) 6331–6347.
[10] C. Wang, Z. Peng, Y. Liu, S. Li, Z. Zhao, W. Chen, Q. Wang, Q. M, Two-dimensional symmetrical radial sub-aperture coherence and the local precision defect elimination method for high-precision beam steering, Opt. Express 27 (13) (2019) 18751–18765.
[11] C. Wang, W. Chen, Z. Zhao, Q. Mu, Q. Wang, Quantitative error analysis for non-mechanical phase-controlled beam steering based on symmetrical radial sub-aperture coherence algorithm, Liq. Cryst. 48 (3) (2020) 1–7.
[12] A.K. Kirby, G.D. Love, Fast, large and controllable phase modulation using dual frequency liquid crystals, Opt. Express 12 (7) (2004) 1470–1475.
[13] D. Dayton, S. Browne, J. Gonglewski, S. Restaino, Characterization and control of a multielement dual-frequency liquid-crystal device for high-speed adaptive optical wave-front correction, Appl. Opt. 40 (15) (2001) 2345–2355.
[14] H. Chen, M. Hu, F. Peng, J. Li, Z. An, S. Wu, Ultra-low viscosity liquid crystal materials, Opt. Mater. Expr 5 (3) (2005) 655–660.
[15] R.W. Gerchberg, W.O. Saxton, A practical algorithm for the determination of phase from image and diffraction plane pictures, Optik 35 (1972) 237–250.
[16] P. Netrapalli, P. Jain, S. Sanghavi, Phase retrieval using alternating minimization, IEEE Trans. Signal Process. 63 (18) (2015).

[17] J. Miao, D. Sayre, H.N. Chapman, Phase retrieval from the magnitude of the Fourier transforms of nonperiodic objects, J. Opt. Soc. Amer. A 15 (6) (1998) 1662–1669.
[18] J.R. Fienup, Phase-retrieval algorithms for a complicated optical system, Appl. Opt. 32 (10) (1993) 1737–1746.
[19] M. Yang, Z. Kong, Q. Tan, G. Ren, L. Xue, Precise design of diffraction optical elements based on annular beam shaping, Acta Opt. Sin. 39 (3) (2019) 0305002.
[20] W. Qu, H. Gu, Q. Tan, G. Jin, Precise design of two-dimensional diffractive optical elements for beam shaping, Appl. Opt. 54 (21) (2015) 6521–6525.
[21] X. Deng, Y. Li, Q. Yue, D. Fan, Phase-mixture algorithm applied to design of pure phase elements, Chin. J. Lasers B 4 (005) (1995) 447.
[22] S. Tao, W. Yu, Beam shaping of complex amplitude with separate constraints on the output beam, Opt. Express 23 (2) (2015) 1052–1062.
[23] D. Palima, V.R. Daria, Holographic projection of arbitrary light patterns with a suppressed zero-order beam, Appl. Opt. 46 (20) (2007) 4197–4201.
[24] G. Milewski, D. Engström, J. Bengtsson, Diffractive optical elements designed for highly precise far-field generation in the presence of artifacts typical for pixelated spatial light modulators, Appl. Opt. 46 (1) (2007) 95–105.
[25] Z. Hao, J. Xie, J. Liu, Y. Wang, Elimination of a zero-order beam induced by a pixelated spatial light modulator for holographic projection, Appl. Opt. 48 (30) (2009) 5834–5841.
[26] R. Szweda, Vcsel applications diversify as technology matures, III-Vs Review 19 (1) (2006) 34–38.
[27] J. Kim, A.C. Oh, A. Escuti, A.L. Hosting, S. Seratib, Wide-angle nonmechanical beam steering using thin liquid crystal polarization gratings, Proc. SPIE - the Int. Soc. Opt. Eng 7093 (2008) 709302–709312.